PHYSICAL REVIEW RESEARCH 7, L032043 (2025)

Letter | Editors' Suggestion

Scaling of pseudospectra in exponentially sensitive lattices

Ioannis Kiorpelidis and Konstantinos G. Makris
Department of Physics, University of Crete, 70013 Heraklion, Greece
and Institute of Electronic Structure and Laser (IESL), FORTH, 71110 Heraklion, Greece

(Received 11 September 2024; revised 24 January 2025; accepted 1 May 2025; published 22 August 2025)

One of the important features of non-Hermitian Hamiltonians is the existence of a unique type of singularities, the so-called exceptional points (EPs). When the corresponding systems operate around such singularities, they exhibit ultrasensitive behavior that has no analog in conservative systems. An alternative way to realize such ultra-sensitivity relies on asymmetric couplings. Here we provide a comprehensive analysis based on pseudospectra, that shows the origin of exponential sensitivity, without relying on topological zero modes or the localization of all eigenstates (skin effect), but on the underlying extreme lattice non-normality. In particular, we consider four different types of lattices (Hatano-Nelson, Sylvester-Kac, non-Hermitian Su-Schrieffer-Heeger and a non-Hermitian random lattice) and identify the conditions for exponential sensitivity as a function of the lattice size. Complex and structured pseudospectra reveal the signatures of exponential sensitivity both on the eigenvalue spectra and on the underlying dynamics. Our study, may open new directions on studies related to the exploitation of non-normality for constructing ultra-sensitive systems that do not rely on the existence of EPs.

DOI: 10.1103/PhysRevResearch.7.L032043

Introduction. One of the cornerstones of non-Hermitian physics [1], is the existence of the so-called exceptional points (EPs) [2,3]. Unlike conservative problems, where symmetries cause only eigenvalue degeneracy, here both eigenvalues and eigenmodes coalesce at specific control parameter values. The main physical consequence of eigenstate coalescence is the fact that weak perturbations can dramatically impact the system's response, which depends nonlinearly (algebraically) on the perturbation strength, in contrast to the Hermitian case where the dependence is linear. This characteristic property of EPs has been studied in various contexts from mathematical physics to microwave cavities [4,5]. But their true potential has been reached in the framework of parity-time symmetric [6] and non-Hermitian photonics [7–12], where EPs have been experimentally realized and led to various applications, such as ultrasensitive microresonators [13–16], exceptional point gyroscopes [17], and single mode nanolasers [18], to name a few.

Another intriguing effect, characteristic of non-Hermitian Hamiltonians, is the non-Hermitian skin effect (NHSE) [19–21], which is a direct outcome of nonsymmetric coupling between adjacent elements. This asymmetry is another alternative way to physically implement non-Hermiticity, with the other being the spatial combination of gain-loss materials. Counterintuitively, all the eigenmodes of such periodic systems are localized on one lattice end for Dirichlet boundary conditions. Such localization stems from the fact that any periodic lattice can be mapped to a Hatano-Nelson array under an imaginary gauge transformation [22,23]. NHSE has been extensively studied not only in the framework of Hatano-Nelson Hamiltonians, but also in other lattice systems that exhibit asymmetric couplings. The experimental realization of Hatano-Nelson lattices was elusive for long time due to the difficulty of realizing asymmetric couplings. Nevertheless, the NHSE was recently experimentally demonstrated in various photonic systems, like microring optical cavities, coupled optical fiber loop networks and mode locked lasers [24–27].

The latter studies regarding the NHSE (off-diagonal asymmetry), along with the initial ones regarding the spatial combination of gain-loss materials (on-diagonal complex elements), have established the framework of non-Hermitian photonics, where non-Hermiticity can be realized based on these two different methodologies. The synergy of non-Hermiticity with other physical effects, such as topological bands or optical nonlinearity, has widened the context of non-Hermitian photonics on both theoretical [28,29] and experimental fronts [30–32].

Similar to EPs, the NHSE provides an alternative way to realize ultrasensitive devices based on asymmetric couplings [33–39]. In this regard, the exponential sensitivity associated with NHSE is attributed to its underlying topological nature [34], and has been recently experimentally demonstrated [40–43]. In fact, the eigenspectrum of the problem changes dramatically depending on the boundary conditions, namely closed or periodic. So far all relevant studies devoted to topological sensors and topological amplification rely on perturbation theory and are strictly focused on the sensitivity of the zero eigenmode, by examining various mathematical sensitivity metrics such as energy shifts and condition numbers [39], for example.

In this paper, we investigate the effect of exponential sensitivity beyond its topological context and the NHSE. In particular, we apply the theory of pseudospectra [44], which, outside the fields of applied mathematics, fluid mechanics

Published by the American Physical Society under the terms of the Creative Commons Attribution 4.0 International license. Further distribution of this work must maintain attribution to the author(s) and the published article's title, journal citation, and DOI.

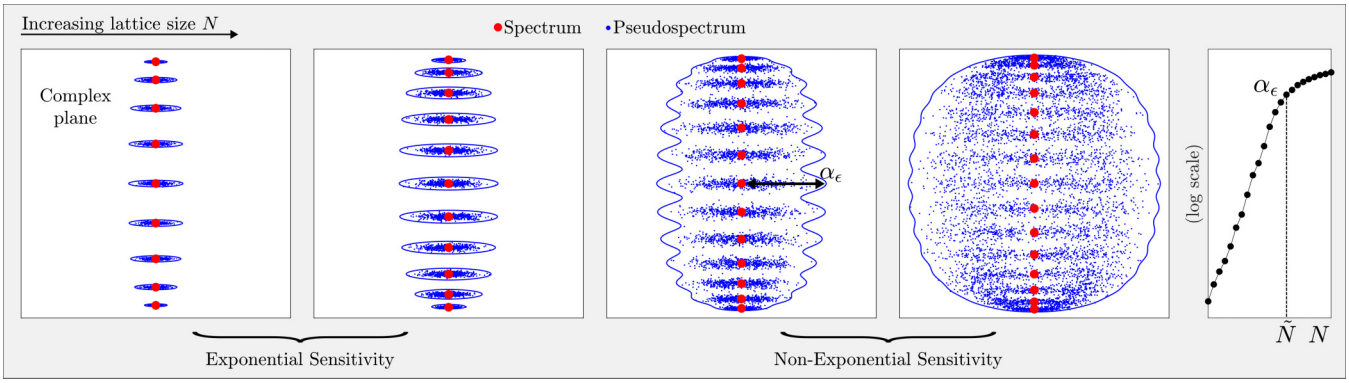


FIG. 1. Schematic of complex pseudospectrum scaling with the lattice size N. For small N's, the pseudospectrum (blue dots) consists of N disks-clouds centered around the eigenvalues (red dots). By increasing N, the pseudospectrum extends in the complex plane and beyond a critical value $\tilde{N}$ it forms a single cloud. The abscissa α_ϵ measures the extend of the pseudospectrum: it grows exponentially with N up to $\tilde{N}$.

[45,46], and a few studies on excess noise in laser cavities [47,48], remains largely unknown in physics. Despite this, pseudospectra have been introduced in the context of non-Hermitian optics, as they unify the concepts of spectral sensitivity and power dynamics [49–52]. Furthermore, they offer a mathematically rigorous foundation for describing a range of problems involving topology and driven systems [53–55], making them particularly relevant in non-Hermitian physics. Our results reveal two different aspects: From the mathematical point of view, the application of pseudospectra theory in this context allows us to move beyond perturbation theory and unify the spectral and dynamical sensitivity. From the physical point of view, which is our focus, the pseudospectra theory reveals the critical values of lattice size, of perturbation strength and of device length, that determine whether we have exponential sensitivity or not. We consider different tight-binding lattices with asymmetric nearest-neighbor hopping terms, like the Hatano-Nelson (HN) [22], Sylvester-Kac (SK) [56,57], non-Hermitian Su-Schrieffer-Heeger (NH-SSH) model [58,59], and a disordered lattice with random coupling coefficients. We study the scalings of complex [44] and structured pseudospectra [60–62] with the lattice size N, and find that the pseudospectral abscissa α_ϵ and the maximum power growth exhibit exponential sensitivity with N, implying that tuning this parameter is crucial for practical sensing applications. Figure 1 illustrates how the pseudospectrum depends on N and also shows the determination of α_ϵ along with its variation with N.

Non-Hermitian lattices. Let us start by presenting in Figs. 2(a)–2(d) the four discrete lattices that we consider in our study. The wave evolution is governed by the coupled mode equation of paraxial optics for the electric field's envelope amplitudes-$\boldsymbol{\psi}$, namely $\dot{\boldsymbol{\psi}} = -i\mathbf{H}\boldsymbol{\psi}$, with $\boldsymbol{\psi}(t=0) = \boldsymbol{\psi}_0$, where dot denotes differentiation with respect to time t (for cavities) or propagation distance (for waveguides), $\mathbf{H}$ the Hamiltonians of the models, and $\boldsymbol{\psi}_0$ the initial conditions. The Hamiltonians can all be written in the following form: $\mathbf{H} = -\sum_{n=1}^{N-1}(J_n|n\rangle\langle n+1| + \tilde{J}_n|n+1\rangle\langle n|)$, where $|n\rangle$ is the basis state localized at lattice site n, J_n is the hopping amplitude for transitions from site $n+1$ to site n ($n = 1, \ldots, N$), and $\tilde{J}_n$ is the hopping amplitude in the reverse direction. In the Hatano-Nelson model $J_n = J_L$ and $\tilde{J}_n = J_R$ $\forall n$, in the Sylvester-Kac $J_n = cn/N$ and $\tilde{J}_n = c(N-n)/N$, in the SSH $J_n = J_L$ and $\tilde{J}_n = J_R$ for odd n and $J_n = \tilde{J}_n = J$ for even n, and in the random model J_n and $\tilde{J}_n$ are random numbers uniformly distributed in $[0, h]$.

Due to the asymmetry of the hopping terms, $J_n \neq \tilde{J}_n$, the Hamiltonians $\mathbf{H}$ exhibit different right and left eigenvectors, $\boldsymbol{\psi}_n^R$ and $\boldsymbol{\psi}_n^L$ respectively, $n = 1, 2, \ldots, N$, with distinct spatial profiles; see Supplemental Material (SM) [63]. We note here that in all models, we can find at least one pair of right/left eigenstates which are localized at opposite lattice edges (for the random model we have selected a realization that satisfies this property) and thus their spatial overlap depends exponentially on the lattice size.

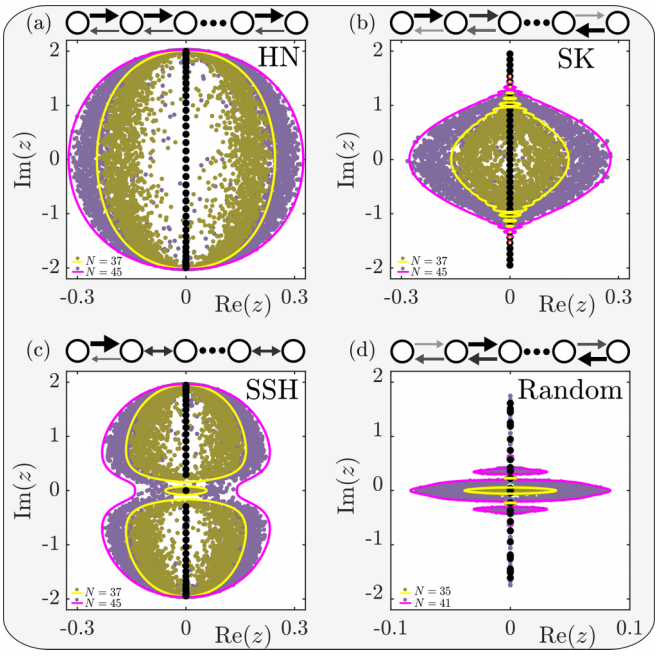


FIG. 2. (a)−(d) Eigenspectra on the complex plane $z \in \mathbb{C}$ (black dots) and complex pseudospectra of the matrix $\mathbf{A} = -i\mathbf{H}$, for $\epsilon = 10^{-5}$ and for two lattice sizes N (purple and yellow dots/lines). (a) Hatano-Nelson model ($J_R = 3/2$, $J_L = 2/3$), (b) Sylvester-Kac model ($c = 2$), (c) Non-Hermitian Su-Schrieffer-Heeger model ($J_R = 1.8$, $J_L = 0.4$, $J = 1.1$) and (d) Random asymmetric model (hopping terms J_n and $\tilde{J}_n$ uniformly in [0,2]).

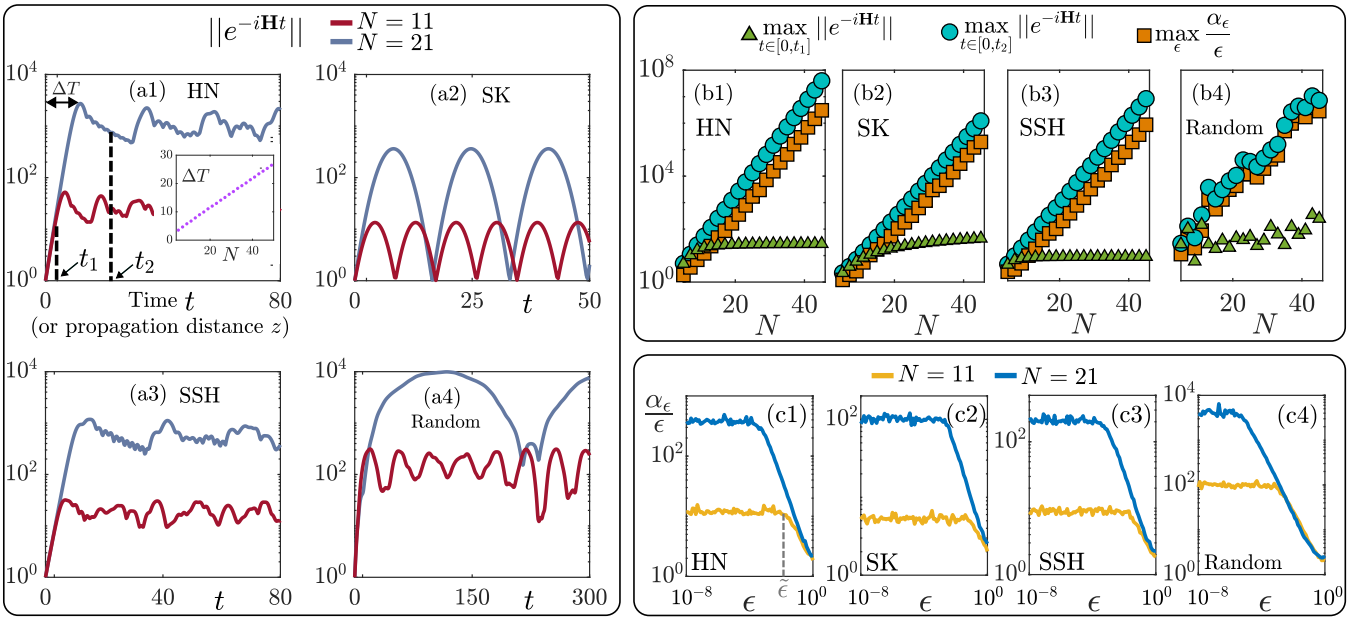


FIG. 3. Scaling of spectral and dynamical sensitivity based on complex pseudospectra. (a1)–(a4) Time-evolution of the propagator norm for two lattice sizes ($N = 11$ and $N = 21$). Inset in (a1): The time ΔT scales linearly with N. (b1)–(b4) Shown are the $\max_{t\in[0,t_1]} ||e^{-i\mathbf{H}t}||$ for $t_1 \ll 1$, the $\max_{t\in[0,t_2]} ||e^{-i\mathbf{H}t}||$ for $t_2 \gg 1$, and the Kreiss constant $\max_\epsilon(\alpha_\epsilon/\epsilon)$. The first quantity does not scale exponentially with N, whereas the latter two do. In (b1) $t_1 = 4$, in (b2) $t_1 = 2.5$, in (b3) $t_1 = 3$ and in (b4) $t_1 = 10$. In all panels $t_2 = 800$. (c1)–(c4) Variation of α_ϵ/ϵ with ϵ, for two different lattice sizes ($N = 11$ and $N = 21$). The abscissa grows linearly up to a value $\tilde{\epsilon}$, while beyond $\tilde{\epsilon}$ it scales as $\alpha_\epsilon \sim \epsilon^\delta$. The value of the abscissa at $\tilde{\epsilon}$ is an estimate for ΔT.

The solution of the coupled mode equations is given by $\boldsymbol{\psi}(t) = e^{-i\mathbf{H}t}\boldsymbol{\psi}_0$, where the matrix $e^{-i\mathbf{H}t}$ is refereed as the propagator or evolution matrix [44]. The quantity $||\boldsymbol{\psi}(t)||^2$ is a measurable observable of the system called the optical power and therefore the ratio $||\boldsymbol{\psi}(t)||/||\boldsymbol{\psi}_0||$ is the square root of the amplification ratio of the lattice [50,51]. In all the considered lattices, the eigenvalue spectra $\{E_n\}$, denoted by $\sigma(\mathbf{H})$, are purely real regardless of whether N is even or odd, since $\mathbf{H}$ can be mapped to a Hermitian Hamiltonian by applying a similarity transformation (see SM). The solution $\boldsymbol{\psi}(t)$ written in the right eigenbasis $\{\boldsymbol{\psi}_n^R\}$ of $\mathbf{H}$ takes the form, $\boldsymbol{\psi}(t) = \sum_{n=1}^N c_n e^{-iE_n t}\boldsymbol{\psi}_n^R$, where the c_n coefficients can be uniquely determined by the initial conditions $\boldsymbol{\psi}_0$. The eigenvalues E_n are purely real (despite the non-Hermiticity of the matrix), and therefore the Euclidean norms $||\boldsymbol{\psi}(t)||$ are bounded in time. In fact, the Hamiltonians $\mathbf{H}$ of the considered models are non-normal, i.e. $[\mathbf{H}, \mathbf{H}^\dagger] \neq 0$, and due to this any initial condition can, in principle, be amplified, in the sense that $||\boldsymbol{\psi}(t)||$ can exceed $||\boldsymbol{\psi}_0||$. In other words, the optical power $\sum_n |\psi_n|^2$ is not a conserved quantity anymore but oscillates [50,51].

Complex pseudospectra. In order to systematically explore these power oscillations, we will apply the pseudospectra theory [44]. In this paragraph, we provide the simplest definition of complex pseudospectrum. Given any $\epsilon > 0$, the pseudospectrum $\sigma_\epsilon(\mathbf{A})$ of a matrix $\mathbf{A}$ is the set of complex numbers z that are eigenvalues of perturbed matrices $\mathbf{A} + \mathbf{E}$, with $\mathbf{E}$ being a complex random matrix, whose 2-matrix norm is less than ϵ [64]. Strictly speaking the definition is: $\sigma_\epsilon(\mathbf{A}) = \bigcup_{||\mathbf{E}||<\epsilon} \sigma(\mathbf{A} + \mathbf{E})$. We present our results regarding the complex pseudospectra of the four lattices in Fig. 2. More specifically, in Figs. 2(a)–2(d) we show the spectra (black dots) of the matrix $\mathbf{A} = -i\mathbf{H}$, as well as, the corresponding pseudospectra by computing 100 perturbed matrices $\mathbf{A} + \mathbf{E}$ for $\epsilon = 10^{-5}$, and for two different lattice sizes N (yellow and purple dots, respectively). Notice that the pseudospectrum $\sigma_\epsilon(\mathbf{A})$ forms a cloud of eigenvalues around the spectrum $\sigma(\mathbf{A})$ and its boundary [solid lines shown in Figs. 2(a)–2(d)] is determined by an equivalent pseudospectrum definition based on the resolvent of $\mathbf{A}$ (see SM).

Scaling of complex pseudospectra with N. Regarding the spectral sensitivity, Fig. 1 presents a schematic depiction of the general behavior of all the four lattices that we consider. In particular, for small N's, the pseudospectrum consists of N disks-clouds centered at the N eigenvalues of $\mathbf{A}$. As N increases, the radii of these disks grow, and beyond a certain value $\tilde{N}$, they merge into a single-cloud. A metric for the extent of the pseudospectrum is provided by the pseudospectral abscissa, $\alpha_\epsilon = \max \mathrm{Re}[\sigma_\epsilon(\mathbf{A})]$, which also provides a measure of the lattice's spectral sensitivity. The right panel of Fig. 1 shows the variation of α_ϵ with N: notice that it increases exponentially up to $\tilde{N}$, corresponding to the onset of the single-cloud regime.

Regarding the dynamical sensitivity of the lattice, a measure quantifying the power dynamics is the maximum growth at any given time t, $\max_{\boldsymbol{\psi}_0, ||\boldsymbol{\psi}_0||=1} ||\boldsymbol{\psi}(t)||/||\boldsymbol{\psi}_0||$. By definition, the latter quantity is equal to the 2-norm of the propagator matrix, which in turn is equal to its maximum singular value. Shown in Figs. 3(a1)–3(a4) is the time evolution of the propagator norm for all models. Despite the real spectrum of $\mathbf{H}$, amplification occurs ($||e^{-i\mathbf{H}t}|| > 1$) because $\mathbf{H}$ is non-normal. Interestingly, for large times $t_2 \gg 1$, the max-

imum power growth scales exponentially with the lattice size N. Let us note here that this exponential dependence is not constrained by a critical value of N, highlighting the distinction between exponential spectral sensitivity—bounded by a critical value $\tilde{N}$—and dynamical exponential sensitivity. This is illustrated in Figs. 3(b1)–3(b4) where the $\max_{t\in[0,t_2]} ||e^{-i\mathbf{H}t}||$ is displayed. On the contrary, for small times $t_1 \ll 1$, the $\max_{t\in[0,t_1]} ||e^{-i\mathbf{H}t}||$ does not scale exponentially with N. The corresponding time scale ΔT after which the lattice displays exponential sensitivity, scales linearly with N [see the inset of Fig. 3(a1)]. The pseudospectrum renders back information regarding the exponential sensitivity of the power dynamics through the Kreiss matrix theorem [44] $\mathcal{K}(\mathbf{A}) \leqslant \max_t ||e^{\mathbf{A}t}|| \leqslant eN\mathcal{K}(\mathbf{A})$, where e is the Euler's number and $\mathcal{K}(\mathbf{A}) = \max_{\epsilon>0}(\alpha_\epsilon/\epsilon)$ is the Kreiss constant. Figures 3(b1)–3(b4) show that $\mathcal{K}(\mathbf{A})$ increases exponentially with N.

Scaling of complex pseudospectra with ϵ. In this paragraph, we are interested to see the scaling of the pseudospectral abscissa α_ϵ of $\mathbf{A}$, by keeping N constant and varying the perturbation parameter ϵ. We present our results in Figs. 3(c1)–3(c4). Notice that α_ϵ increases linearly up to a value $\tilde{\epsilon}$, and for higher values it scales as $\alpha_\epsilon \sim \epsilon^\delta$. In SM we show that the exponent δ converges to $1/N$ for large asymmetry between right and left couplings, suggesting that the lattice exhibits the same sensitivity with that of an exceptional point of order N. This scaling of the pseudospectral abscissa is independent of the lattice size N, yet the value $\tilde{\epsilon}$ decreases with increasing N. Let us make a comment at this point: The pseudospectrum expands in the complex plane, not only by increasing the lattice size N as is shown in Figs. 1 and 2, but also by increasing the perturbation parameter ϵ. As the perturbation parameter ϵ increases, the pseudospectrum expands in the complex plane as well, and a similar transition from N disks-clouds to a single-cloud occurs. This transition takes place at the critical value $\tilde{\epsilon}$. Moreover, the value of $1/\alpha_\epsilon$ at $\tilde{\epsilon}$ offers estimate for the time scale ΔT [44] after which the lattice supports exponential sensitivity with N.

Scaling of structured pseudospectra with N. As stated before, the abscissa α_ϵ of the complex pseudospectrum scales exponentially with the lattice size N, up to a critical value $\tilde{N}$. Such a scaling, however, involves a perturbation matrix $\mathbf{E}$ of which all elements are generally nonzero—it affects all entries of the Hamiltonian—making it unsuitable for studying the sensitivity of the lattices's spectra under experimentally realistic perturbations. The latter analysis can instead be performed with the structured pseudospectrum [60–62]: the structured pseudospectrum of a matrix $\mathbf{A}$, denoted as $\sigma_\epsilon^{\mathrm{Str}}(\mathbf{A})$, is defined analogously to the complex pseudospectrum with the difference that the random matrix $\mathbf{E}$ exhibits specific structure, $\sigma_\epsilon^{\mathrm{Str}}(\mathbf{A}) = \bigcup_{\mathbf{E}-\mathrm{Structured},||\mathbf{E}||<\epsilon} \sigma(\mathbf{A}+\mathbf{E})$. For instance, $\mathbf{E}$ may have nonzero elements exclusively on its diagonal, suggesting that only the onsite potential of the lattice is perturbed (see SM for more details and illustrations of the structured pseudospectrum).

When the Hamiltonian $\mathbf{H}$ is subject to a single-element perturbation [Fig. 4(a)], it is implied that two lattice sites get connected. Figures 4(b1)–4(b4) illustrate how perturbing four distinct elements of $\mathbf{H}$ leads to the corresponding four lattice configurations. Moreover, as can be seen in Figs. 4(c1)–4(c4), the $\alpha_\epsilon^{\mathrm{Str}}$ scales exponentially with the system size N when

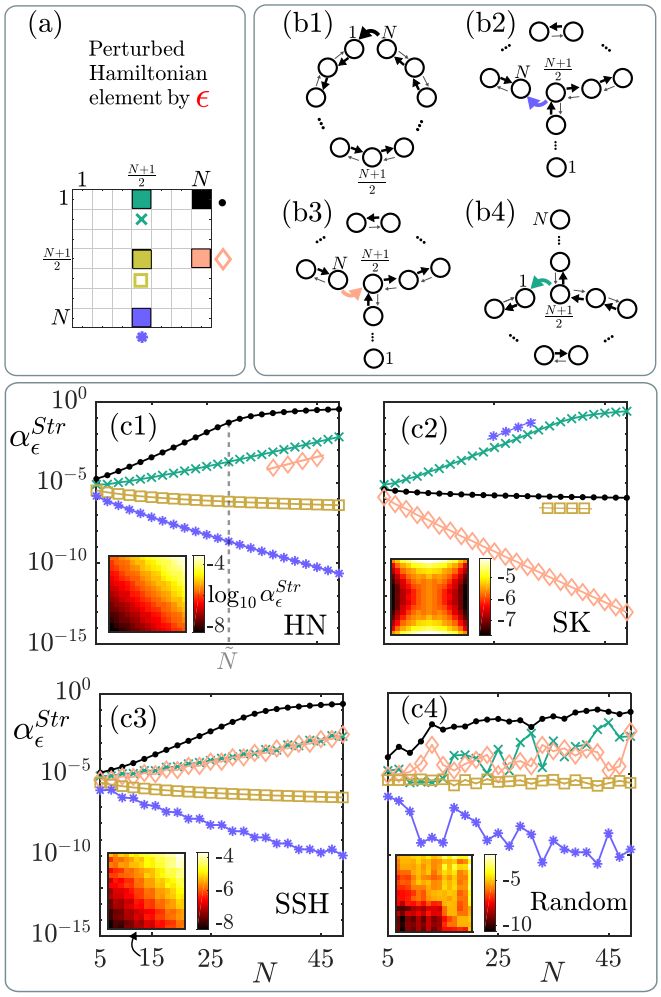


FIG. 4. Scaling of spectral sensitivity with N, based on the structured pseudospectra. (a) The matrix denotes five different elements of $\mathbf{H}$ that are perturbed by a complex random number of ϵ magnitude. (b1)–(b4) Different geometrical configurations resulting from the perturbation of different Hamiltonian elements denoted in (a). (c1)–(c4) Variation of the structured pseudospectral abscissa $\alpha_\epsilon^{\mathrm{Str}}$ with N, when each one of the five different elements of $\mathbf{H}$ denoted in (a) is perturbed. ϵ is set at 10^{-5}. The insets matrices illustrate which Hamiltonian element demonstrates the highest sensitivity when perturbed.

perturbing appropriate Hamiltonian elements. Based on the structured pseudospectra technique, we can identify which element results to the most sensitive response of the whole system. For instance, for the inset plots of Figs. 4(c1)–4(c4), we kept both ϵ and N fixed ($\epsilon = 10^{-5}$ and $N = 15$), we considered single element perturbation matrices $\mathbf{E} = \epsilon\delta_{n,m}$ with $n, m = 1, \ldots, 15$, and we computed the value of the structured abscissa (color bar) for each pair (n, m). At this point, we should stress the difference between the structured pseudospectrum approach and the conventional perturbation methods [34]. In the latter ones, the focus is on the energy shift of one individual zero-energy mode under applied perturbations, whereas in the former one, the collective effect of all eigenvalues is taken into account.

Discussion and Conclusions. In summary, we have presented a scaling analysis of pseudospectra in exponential sensitive lattices. In particular, we considered four different examples of coupled optical elements (cavities or waveguides) that have asymmetric coupling coefficients. On one hand, the scaling of complex pseudospectra (of both the unperturbed and perturbed Hamiltonian) provides us useful information about the power dynamics scaling with the system's size N. Moreover, additional scaling with respect to the perturbation strength ϵ, gives us an understanding of the limits of this exponential sensitivity. On the other hand, scaling of the structured pseudospectra offers valuable information regarding the sensitivity of the spectrum, again with respect to N.

Unlike all previous works, we do not rely on topological effects driven from the extreme sensitivity on boundary conditions, but we focus on characterizing the underlying nonnormality. Let us note here the strengths of pseudospectra: (a) the computation of eigenvalue spectra could be numerically much more efficient, both in terms of computational cost and stability than the computation of the matrix exponentials. Thus, especially for problems involving large matrices (for example quantum problems) the pseudospectra could offer a significant advantage. (b) Perturbation theory focuses on the impact of a perturbation on individual eigenvalues, while the pseudospectrum reveals the collective impact of a perturbation on all eigenvalues; it provides a global perspective. This global framework can be utilized by machine learning to design ultrasensitive structures.

In conclusion, while recent experiments in non-Hermitian photonics have demonstrated asymmetric optical lattices [24,25,27,41], the realization of exponential sensitivity in power dynamics, as well as, its demonstration in nontopological lattices remains an open problem. Such a demonstration could, in principle, be achieved through discrete-time quantum walks of optical pulses in coupled fiber loops [24]. Thus, our results may pave the way for efficient design of ultrasensitive devices without relying on higher-order exceptional points.

Acknowledgments. K.G.M. acknowledges enlightening discussions with Professsor C. Lubich during the workshop "Nonlinear Optics: Physics, Analysis, and Numerics" at Mathematisches Forschungsinstitut Oberwolfach (11–15 March 2024), regarding the structured pseudospectra. This project was funded by the European Research Council (ERC-Consolidator) under Grant Agreement No. 101045135 (Beyond_Anderson).

[1] N. Moiseyev, *Non-Hermitian Quantum Mechanics* (Cambridge University Press, New York, 2011).
[2] W. D. Heiss, Exceptional points of non-Hermitian operators, J. Phys. A **37**, 2455 (2004).
[3] M. V. Berry, Physics of nonHermitian degeneracies, Czech. J. Phys. **54**, 1039 (2004).
[4] T. Stehmann, W. D. Heiss, and F. G. Scholtz, Observation of exceptional points in electronic circuits, J. Phys. A **37**, 7813 (2004).
[5] C. Dembowski, H. D. Gräf, H. L. Harney, A. Heine, W. D. Heiss, H. Rehfeld, and A. Richter, Experimental observation of the topological structure of exceptional points, Phys. Rev. Lett. **86**, 787 (2001).
[6] C. M. Bender and S. Boettcher, Real spectra in non-Hermitian Hamiltonians having PT symmetry, Phys. Rev. Lett. **80**, 5243 (1998).
[7] R. El-Ganainy, K. G. Makris, D. N. Christodoulides, and Z. H. Musslimani, Theory of coupled optical *PT*-symmetric structures, Opt. Lett. **32**, 2632 (2007).
[8] K. G. Makris, R. El-Ganainy, D. N. Christodoulides, and Z. H. Musslimani, Beam dynamics in $\mathcal{PT}$ symmetric optical lattices, Phys. Rev. Lett. **100**, 103904 (2008).
[9] Z. H. Musslimani, K. G. Makris, R. El-Ganainy, and D. N. Christodoulides, Optical solitons in $\mathcal{PT}$ periodic potentials, Phys. Rev. Lett. **100**, 030402 (2008).
[10] K. G. Makris, R. El-Ganainy, D. N. Christodoulides, and Z. H. Musslimani, $\mathcal{PT}$-symmetric optical lattices, Phys. Rev. A **81**, 063807 (2010).
[11] A. Guo, G. J. Salamo, D. Duchesne, R. Morandotti, M. Volatier-Ravat, V. Aimez, G. A. Siviloglou, and D. N. Christodoulides, Observation of $\mathcal{PT}$-symmetry breaking in complex optical potentials, Phys. Rev. Lett. **103**, 093902 (2009).
[12] C. E. Rüter, K. G. Makris, R. El-Ganainy, D. N. Christodoulides, M. Segev, and D. Kip, Observation of parity-time symmetry in optics, Nat. Phys. **6**, 192 (2010).
[13] J. Wiersig, Sensors operating at exceptional points: General theory, Phys. Rev. A **93**, 033809 (2016).
[14] J. Wiersig, Enhancing the sensitivity of frequency and energy splitting detection by using exceptional points: Application to microcavity sensors for single-particle detection, Phys. Rev. Lett. **112**, 203901 (2014).
[15] H. Hodaei, A. U. Hassan, S. Wittek, H. Garcia-Gracia, R. El-Ganainy, D. N. Christodoulides, and M. Khajavikhan, Enhanced sensitivity at higher-order exceptional points, Nature (London) **548**, 187 (2017).
[16] W. Chen, Ş. K. Özdemir, G. Zhao, J. Wiersig, and L. Yang, Exceptional points enhance sensing in an optical microcavity, Nature (London) **548**, 192 (2017).
[17] M. P. Hokmabadi, A. Schumer, D. N. Christodoulides, and M. Khajavikhan, Non-Hermitian ring laser gyroscopes with enhanced Sagnac sensitivity, Nature (London) **576**, 70 (2019).
[18] H. Hodaei, M. A. Miri, M. Heinrich, D. N. Christodoulides, and M. Khajavikhan, Parity-time–symmetric microring lasers, Science **346**, 975 (2014).
[19] T. E. Lee, Anomalous edge state in a non-Hermitian lattice, Phys. Rev. Lett. **116**, 133903 (2016).
[20] X. Zhang, T. Zhang, M. H. Lu, and Y. F. Chen, A review on non-Hermitian skin effect, Adv. Phys. **7**, 2109431 (2022).
[21] V. M. Martinez Alvarez, J. E. Barrios Vargas, and L. E. F. Foa Torres, Non-Hermitian robust edge states in one dimension: Anomalous localization and eigenspace condensation at exceptional points, Phys. Rev. B **97**, 121401(R) (2018).
[22] N. Hatano and D. R. Nelson, Localization transitions in non-Hermitian quantum mechanics, Phys. Rev. Lett. **77**, 570 (1996).
[23] N. Hatano and D. R. Nelson, Vortex pinning and non-Hermitian quantum mechanics, Phys. Rev. B **56**, 8651 (1997).

[24] S. Weidemann, M. Kremer, T. Helbig, T. Hofmann, A. Stegmaier, M. Greiter, R. Thomale, and A. Szameit, Topological funneling of light, Science **368**, 311 (2020).
[25] Y. G. N. Liu, Y. Wei, O. Hemmatyar, G. G. Pyrialakos, P. S. Jung, D. N. Christodoulides, and M. Khajavikhan, Complex skin modes in non-Hermitian coupled laser arrays, Light Sci. Appl. **11**, 336 (2022).
[26] Z. Gao, X. Qiao, M. Pan, S. Wu, J. Yim, K. Chen, B. Midya, L. Ge, and L. Feng, Two-dimensional reconfigurable non-Hermitian gauged laser array, Phys. Rev. Lett. **130**, 263801 (2023).
[27] C. R. Leefmans, M. Parto, J. Williams, G. H. Y. Li, A. Dutt, F. Nori, and A. Marandi, Topological temporally mode-locked laser, Nat. Phys. **20**, 852 (2024).
[28] Z. Gong, Y. Ashida, K. Kawabata, K. Takasan, S. Higashikawa, and M. Ueda, Topological phases of non-Hermitian systems, Phys. Rev. X **8**, 031079 (2018).
[29] K. Kawabata, K. Shiozaki, M. Ueda, and M. Sato, Symmetry and topology in non-Hermitian physics, Phys. Rev. X **9**, 041015 (2019).
[30] S. Weimann, M. Kremer, Y. Plotnik, Y. Lumer, S. Nolte, K. G. Makris, M. Segev, M. Rechtsman, and A. Szameit, Topologically protected bound states in photonic parity–time-symmetric crystals, Nat. Mater. **16**, 433 (2017).
[31] M. Bandres, S. Wittek, G. Harari, M. Parto, J. Ren, M. Segev, D. N. Christodoulides, and M. Khajavikhan, Topological insulator laser: Experiments, Science **359**, eaar4005 (2018).
[32] S. Xia, D. Kaltsas, D. Song, I. Komis, J. Xu, A. Szameit, H. Buljan, K. G. Makris, and Z. Chen, Nonlinear tuning of PT symmetry and non-Hermitian topological states, Science **372**, 72 (2021).
[33] N. Okuma, K. Kawabata, K. Shiozaki, and M. Sato, Topological origin of non-Hermitian skin effects, Phys. Rev. Lett. **124**, 086801 (2020).
[34] J. C. Budich and E. J. Bergholtz, Non-Hermitian topological sensors, Phys. Rev. Lett. **125**, 180403 (2020).
[35] A. McDonald and A. A. Clerk, Exponentially-enhanced quantum sensing with non-Hermitian lattice dynamics, Nat. Commun. **11**, 5382 (2020).
[36] F. Koch and J. C. Budich, Quantum non-Hermitian topological sensors, Phys. Rev. Res. **4**, 013113 (2022).
[37] L. Bao, B. Qi, and D. Dong, Exponentially enhanced quantum non-Hermitian sensing via optimized coherent drive, Phys. Rev. Appl. **17**, 014034 (2022).
[38] R. Zhang and T. Chen, True exponentially enhanced sensing in the non-Hermitian topological phase, Appl. Phys. Lett. **124**, 174002 (2024).
[39] Y. O. Nakai, N. Okuma, D. Nakamura, K. Shimomura, and M. Sato, Topological enhancement of non-normality in non-Hermitian skin effects, Phys. Rev. B **109**, 144203 (2024).
[40] H. Yuan, W. Zhang, Z. Zhou, W. Wang, N. Pan, Y. Feng, H. Sun, and X. Zhang, Non-Hermitian topolectrical circuit sensor with high sensitivity, Adv. Sci. **10**, 2301128 (2023).
[41] M. Parto, C. Leefmans, J. Williams, and A. Marandi, Enhanced sensitivity via non-Hermitian topology, Light Sci. Appl. **14**, 6 (2025).
[42] L. Bao, B. Qi, F. Nori, and D. Dong, Exponential sensitivity revival of noisy non-Hermitian quantum sensing with two-photon drives, Phys. Rev. Res. **6**, 023216 (2024).
[43] A. Maddi, Y. Aurégan, G. Penelet, V. Pagneux, and V. Achilleos, Exact analog of the Hatano-Nelson model in one-dimensional continuous nonreciprocal systems, Phys. Rev. Res. **6**, L012061 (2024).
[44] L. N. Trefethen and M. Embree, *Spectra and Pseudospectra* (Princeton University Press, Princeton, 2005).
[45] L. N. Trefethen, A. E. Trefethen, S. C. Reddy, and T. A. Driscoll, Hydrodynamic stability without eigenvalues, Science **261**, 578 (1993).
[46] P. J. Schmid, Nonmodal stability theory, Annu. Rev. Fluid Mech. **39**, 129 (2007).
[47] S. Longhi and P. Laporta, Excess noise in intracavity laser frequency modulation, Phys. Rev. E **61**, R989 (2000).
[48] F. Papoff, G. D'Alessandro, and G. L. Oppo, State dependent pseudoresonances and excess noise, Phys. Rev. Lett. **100**, 123905 (2008).
[49] K. G. Makris, L. Ge, and H. E. Türeci, Anomalous transient amplification of waves in non-normal photonic media, Phys. Rev. X **4**, 041044 (2014).
[50] K. G. Makris, Transient amplification due to non-Hermitian interference of dissipative supermodes, Appl. Phys. Lett. **125**, 011102 (2024).
[51] K. G. Makris, Transient growth and dissipative exceptional points, Phys. Rev. E **104**, 054218 (2021).
[52] I. Komis, D. Kaltsas, S. Xia, H. Buljan, Z. Chen, and K. G. Makris, Robustness versus sensitivity in non-Hermitian topological lattices probed by pseudospectra, Phys. Rev. Res. **4**, 043219 (2022).
[53] N. Okuma and M. Sato, Non-Hermitian topological phenomena: A review, Annu. Rev. Condens. Matter Phys. **14**, 83 (2023).
[54] N. Okuma and M. Sato, Hermitian zero modes protected by nonnormality: Application of pseudospectra, Phys. Rev. B **102**, 014203 (2020).
[55] I. Kiorpelidis, F. K. Diakonos, G. Theocharis, and V. Pagneux, Transient amplification in stable Floquet media, Phys. Rev. B **110**, 134315 (2024).
[56] O. Taussky and J. Todd, Another look at a matrix of Mark Kac, Linear Algebra Appl. **150**, 341 (1991).
[57] G. M. L. Gladwell, T. H. Jones, and N. B. Willms, A test matrix for an inverse eigenvalue problem, J. Appl. Math. **2014**, 1 (2014).
[58] S. Lieu, Topological phases in the non-Hermitian Su-Schrieffer-Heeger model, Phys. Rev. B **97**, 045106 (2018).
[59] S. Yao and Z. Wang, Edge states and topological invariants of non-Hermitian systems, Phys. Rev. Lett. **121**, 086803 (2018).
[60] N. Guglielmi and C. Lubich, Transient dynamics under structured perturbations: Bridging unstructured and structured pseudospectra, SIAM J. Numer. Anal. **63**, 908 (2025).
[61] A. Böttcher, M. Embree, and V. I. Sokolov, The spectra of large Toeplitz band matrices with a randomly perturbed entry, Math. Comput. **72**, 1329 (2003).
[62] S. Graillat, A note on structured pseudospectra, J. Comput. Appl. Math. **191**, 68 (2006).
[63] See Supplemental Material at http://link.aps.org/supplemental/10.1103/PhysRevResearch.7.L032043 for details on the models and additional results and figures supporting the main text.
[64] The matrix 2-norm is defined as $||\mathbf{A}|| = \max_{\boldsymbol{\psi}_0} \frac{||\mathbf{A}\boldsymbol{\psi}_0||}{||\boldsymbol{\psi}_0||}$ where $||\boldsymbol{\psi}_0||$ is the Euclidean norm of the vector $\boldsymbol{\psi}_0$.